TECHNOLOGIES AND ENGINEERING

Journal homepage: https://technologies-engineering.com.ua/en
Vol. 26, No. 3, 2025

Received: 21.01.2025
Revised: 09.05.2025
Accepted: 25.06.2025

UDC 552.576.1:661.183.03:554.723.2
DOI: 10.30857/2786-5371.2025.3.2

Adsorbents derived from nitric acid-oxidised coal and activated with potassium hydroxide

Volodymyr Kucherenko
Doctor of Chemical Sciences, Senior Researcher
L.M. Litvinenko Institute of Physical-Organic and Coal Chemistry
of the National Academy of Sciences of Ukraine
02155, 50 Kharkivske Hwy., Kyiv, Ukraine
https://orcid.org/0000-0001-7234-947X

Yuliia Tamarkina*
PhD in Chemical Sciences, Senior Researcher
L.M. Litvinenko Institute of Physical-Organic and Coal Chemistry
of the National Academy of Sciences of Ukraine
02155, 50 Kharkivske Hwy., Kyiv, Ukraine
https://orcid.org/0000-0002-8747-4481

Anastasiia Redko
Leading Engineer
L.M. Litvinenko Institute of Physical-Organic and Coal Chemistry
of the National Academy of Sciences of Ukraine
02155, 50 Kharkivske Hwy., Kyiv, Ukraine
https://orcid.org/0000-0001-9768-4020

Iryna Frolova
PhD in Chemical Sciences, Researcher
L.M. Litvinenko Institute of Physical-Organic and Coal Chemistry
of the National Academy of Sciences of Ukraine
02155, 50 Kharkivske Hwy., Kyiv, Ukraine
https://orcid.org/0000-0001-9660-5474

Abstract. Alkaline activation is the most effective method for producing carbon-based adsorbents with a highly developed surface area (⩾1,000 m^2/g). However, its major drawback – the requirement for large quantities of alkali – necessitates research aimed at improving the process. This study aimed to quantitatively assess the effect of nitric acid oxidation of long-flame coal on the porous structure and adsorption properties of adsorbents produced by alkaline activation at a low KOH-to-coal ratio (⩽1 g/g). Experimental, analytical and comparative scientific methods were employed. The properties of the adsorbents were characterised using infrared spectroscopy, porometry, and the kinetics and isotherms of 4-chlorophenol, methylene blue dye, and lead cation adsorption from aqueous solutions (at 25°C). It was found that pre-oxidation of the coal with nitric acid introduces ether, ester, phenolic, carboxylic, and nitro groups into the carbon matrix, resulting in a mass increase of up to 16% and significantly influencing the formation of the adsorbents. Increasing the HNO_3-to-carbon ratio from 0 to 1.0 mol/mol reduces the adsorbent yield (from 50.2% to 33.85%), increases the specific surface area (from 1,685 m^2/g to 2,216 m^2/g), and improves adsorption properties by 25%-51%. The dominant portion (~80%) of the effect occurs within the range of ⩽0.4 mol/mol. A comparison of the porous structure characteristics of the adsorbents revealed that oxidation primarily promotes the formation of subnanopores and mesopores with diameters of 2-5 nm. A comparison of adsorption properties showed that adsorbents derived from oxidised coal adsorb greater

---

Suggested Citation:
Kucherenko, V., Tamarkina, Yu., Redko, A., Frolova, I. (2025). Adsorbents derived from nitric acid-oxidised coal and activated with potassium hydroxide. *Technologies and Engineering,* 26(3), 24-37. doi: 10.30857/2786-5371.2025.3.2.

*Corresponding author

quantities of adsorbates (by a factor of 1.20-1.43) and with a higher initial rate (by a factor of 1.2-4.0). This property is particularly important for the rapid removal of highly toxic compounds from water. The adsorbent produced from oxidised coal possesses a more developed surface and a subnanoporous structure, and it exhibits greater adsorption activity than the material derived from non-oxidised coal. Pre-oxidation significantly enhances the adsorption capacity of activated carbon in capturing ecotoxicants from aqueous environments

Keywords: oxicarbon; alkaline thermochemolysis; porous carbon material; pore structure; ecotoxicant adsorption

Introduction

Activated carbon (AC) derived from fossil coal represents a broad group of promising adsorptive materials, characterised by well-developed nanoporous structures, high specific surface area, chemical stability, and electrical conductivity. The combination of these properties enables their application in hydrogen, natural gas, and energy storage (e.g. in supercapacitors), as well as in the removal of pollutants from air and water environments. As of 2025, the most widely used method for producing AC is alkaline activation – thermolysis (700°C-900°C) of the precursor material with potassium hydroxide. This is the only method capable of yielding carbon materials with an extremely high specific surface area (approximately 4,000 m^2/g or more). However, it requires high KOH-to-precursor mass ratios ($R_{KOH} \geqslant 3$ g/g), which represents the main drawback of the process and significantly limits its industrial viability. Consequently, research into producing AC using lower (preferably catalytic) amounts of alkali remains highly relevant.

Global studies of alkaline activation have revealed a general trend: the higher the oxygen content in the precursor, the more developed the porous structure of the resulting AC – particularly at lower R_{KOH} ratios. In other words, a high content of structural oxygen is a key prerequisite for producing AC with a well-developed nanoporous structure using reduced quantities of KOH as the activating agent. Two main approaches exist in this context. The first involves selecting raw materials from the category of solid substances with high oxygen content and strong chemical reactivity towards KOH – typically, certain types of biomass. For example, D. Bergna *et al.* (2022) converted hydrolysis lignin with an oxygen content of [O] = 31.9% into AC with a specific surface area of 928 m^2/g under the following alkaline activation conditions: $R_{KOH} = 1.0$ g/g, 800°C, 1 hour. Under precisely the same activation conditions, M. Li *et al.* (2022) obtained AC with a surface area of 1,225 m^2/g from kraft lignin ([O] = 29.41%), while L.S. Queiroz *et al.* (2020) synthesised AC with a well-developed porous structure (1,462 m^2/g) from biomass ([O] = 47.6%). Perhaps the most impressive result achieved via this approach was the production of AC with a surface area of 2,276 m^2/g from sodium lignosulphonate at $R_{KOH} = 0.4$ g/g (Zhu *et al.*, 2024), which exhibited rapid adsorption of organic dyes.

The second approach involves the immobilisation of structural oxygen in the precursor through pre-oxidation using various reagents, most commonly hydrogen peroxide or nitric acid. S.M. Lee *et al.* (2022) demonstrated that pre-oxidising petroleum coke with hydrogen peroxide increased its oxygen content from 1.4% to 12.4% and enhanced the specific surface area of the resulting AC from 874 m^2/g to 3,159 m^2/g. These results were obtained using a high quantity of activator ($R_{KOH} = 3.0$ g/g) under more severe process conditions (850°C, 1.5 hours). The effectiveness of peroxide oxidation at low KOH-to-precursor ratios ($R_{KOH} \leqslant 1.0$ g/g) remains unexplored, and it is therefore still unclear to what extent pre-oxidation can compensate for the reduced amount of activator. There is also a lack of systematic data on the effect of pre-oxidation with nitric acid on the ability of fossil coal to form AC with a well-developed porous structure when using small amounts of activator ($R_{KOH} \leqslant 1.0$ g/g). Using anthracite as an example, S.-Yi. Lee & R.L. Mahajan (2021) found that HNO_3 oxidatively cleaves aliphatic bonds between crystallites and transforms graphene fragments into graphene oxides, increasing the oxygen content and introducing structural nitrogen, which participates in the formation of the threedimensional AC framework during activation. In a study on the alkaline activation of bituminous coal at different stages of metamorphism, Yu.V. Tamarkina *et al.* (2022) showed that the higher the oxygen content in the raw coal, the greater the development of porosity during activation. In particular, long-flame coal produced AC with the highest specific surface area (1,547 m^2/g) and the greatest adsorption activity for removing ecotoxicants from water (Tamarkina *et al.*, 2020).

This led to the task of assessing the extent to which nitric acid oxidation affects the porous structure and adsorption properties of AC derived from long-flame coal. A review of the literature revealed no available data on this subject. The aim of the present study was to determine how pre-oxidation of longflame coal with nitric acid influences the development of the porous structure and adsorption characteristics of carbon materials synthesised by alkaline thermochemolysis under low KOH-to-coal mass ratio conditions (1 g/g).

Materials and Methods

The study used a sample of long-flame coal (grade D according to the Ukrainian fossil coal classification system, DSTU 3472-96, 2009) with a particle size of 0.16-0.25 mm. The sample was characterised by a moisture content of 10.9%, ash content of 1.8%, and volatile matter yield of 44.8%. The elemental composition of the organic coal matter (% daf) was as follows: C – 80.0; H – 5.3; N – 1.9; S – 1.0; O – 11.8 (by difference), where daf (dry ash-free basis) refers to the mass of coal calculated on a dry, ash-free basis. Oxidation of the coal was performed using an aqueous solution of HNO_3 (50%) following the procedure outlined below. A 10 g sample was dried (120 ± 5°C, ⩾ 2 hours), cooled, and mixed with the reagent at a HNO_3-to-carbon ratio (R_{OX}) ranging from 0.1 to 1.0 mol/mol (OX = HNO_3). The mixture was left to stand for 24 hours at room temperature. The oxidised coal product was then filtered and dried to constant weight in a heated oven (120 ± 5°C). The coal mass increase (Δm, %) was determined by comparing the weights before and after oxidation, and the oxidised samples were designated as D_{OX}. The coal was treated with potassium hydroxide by three-stage impregnation: mixing of 10 g of dried coal with 33.3 g of a 30% aqueous KOH solution to achieve a mass ratio of KOH-tocoal (R_{KOH} = 1.0 g/g); holding the mixture for 24 hours at 20°C-30°C; removal of the aqueous phase at 90°C-100°C, followed by drying to constant weight at 120 ± 10°C for at least 2 hours.

The AC samples were obtained by thermoprogrammed alkaline activation, which involved heating the impregnated coal (~40 g) in an argon atmosphere at a rate of 4°C/min to 800°C, maintaining the isothermal condition for 1 hour, and then cooling in an argon flow to a temperature of ⩽50°C. The resulting carbon product was washed to remove potassium compounds (KOH, $KHCO_3$, K_2CO_3) using water, a 0.1 M HCl solution, and water again until no chloride ions were detected (confirmed by $AgNO_3$ test). The samples were then dried at 120 ± 5°C to constant weight. The yield of AC (Y, %) was determined with an accuracy of ±2%. Samples synthesised from raw coal are denoted as AC(D), and those from oxidised coal as AC(D_{OX}).

Infrared (IR) spectra of the coal samples were obtained using pellets made from mixtures of 5% sample and 95% KBr, with 16 scans recorded in the range of 4,000-400 cm^{-1} (PerkinElmer Spectrum RX I FT-IR System). Band assignments were made based on IR spectra of individual organic compounds (Bellamy, 1975). The porous structure characteristics of the AC were determined from nitrogen adsorption-desorption isotherms at low temperature (77 K) using a Micromeritics ASAP 2020 instrument. Prior to measurement, AC samples were degassed for 20 hours at 260°C. The total pore volume, V_t (cm^3/g), was calculated from the volume of N_2 adsorbed at a relative pressure of p/p_0 ~1.0. The specific surface area, S_{BET}, was calculated using the BET method at $p/p_0 \leqslant 0.12$. Integral and differential pore surface area (S_{DFT}, m^2/g) and pore volume (V, cm^3/g) distributions as functions of average pore diameter (D, nm) were calculated using the 2D-NLDFT-HS method (2-Dimensional Nonlocal Density Functional Theory for Heterogeneous Surfaces) in the SAIEUS software (Jagiello *et al.*, 2020). From the integral curves "$V - D$" and "$S_{DFT} - D$", the volumes of ultramicropores (V_{umi}), supermicropores (V_{smi}), subnanopores (V_{1nm}), and micropores (V_{mi}) were determined, where $V_{mi} = V_{umi} + V_{smi}$. The combined volume of mesopores and macropores was calculated as $V_{me+ma} = V_t - V_{mi}$. The margin of error in pore volume determination was ±0.01 cm^3/g. In a similar manner, the specific surface areas of ultramicropores (S_{um}), supermicropores (S_{smi}), subnanopores (S_{1nm}), and micropores (S_{mi}) were determined, as well as the total surface area of mesopores and macropores (S_{me+ma}). The measurement error for specific surface area was ±5%. The classification of pores and their average diameters was adopted according to IUPAC recommendations (Thommes *et al.*, 2015): ultramicropores ($D \leqslant 0.7$ nm), supermicropores ($D = 0.7$-2.0 nm), micropores ($D \leqslant 2.0$ nm). The above categories are collectively referred to as nanopores, with an upper size limit of $D \leqslant 100$ nm. Additionally, the volume fractions (P_V, %) of different pore types in the total adsorptive pore volume, and the surface fractions (P_S, %) of pore types in the total specific surface area (S_{DFT}) of the AC samples were calculated.

Adsorption capacity for selected adsorbates, denoted as A_{AD} (mmol/g), where AD refers to 4chlorophenol (CP), methylene blue dye (MB), or lead(II) cations from a $Pb(NO_3)_2$ solution, was determined as follows. A precisely weighed sample ($m = 0.100$ g) of the AC sample, dried at 120 ± 10°C, was introduced into 100 cm^3 of aqueous adsorbate solution at a predefined initial concentration ($C_{AD(0)}$, mmol/L), and shaken at 25 ± 0.5°C (150 rpm) using a MAXTURDY-45 shaker bath (Daihan). The concentration of AC in the adsorbate solution was kept constant at 1 g/L. After the designated contact time, the mixture was filtered, and either the current concentration, C_{AD} (for adsorption kinetics) or the equilibrium concentration, $C_{AD(e)}$ (for adsorption isotherms), was measured. The concentrations of CP and MB were determined by comparison with calibration curves based on the optical density of the solution, measured using a PerkinElmer Lambda 20 spectrophotometer at wavelengths of 280 nm and 665 nm, respectively (Tamarkina *et al.*, 2022). The concentration of Pb(II) cations was determined by titration with a solution of Trilon B in the presence of xylenol orange as an indicator. The adsorption capacity A_{AD} was calculated using the following formula:

$$A_{AD} = (C_{AD(0)} - C_{AD}) \cdot V/m. \tag{1}$$

Adsorption kinetics data were fitted using the pseudo-first-order (2), pseudo-second-order (3), and intraparticle diffusion (4) models:

$$A_{AD} = A_{AD(e)}[1 - \exp(-k_1\tau)], \tag{2}$$

where k_1 is the rate constant, τ is the adsorption time (Revellame *et al.*, 2020; Wang & Guo, 2022).

$$A_{AD} = k_2 A^2_{AD(e)}\tau / (1 + k_2 A_{AD(e)}\tau), \tag{3}$$

where k_2 is the rate constant, τ is the adsorption time.

$$A_{AD} = k_d\tau^{0.5} + C, \tag{4}$$

where k_d is the rate constant, τ is the adsorption time.
The initial adsorption rate was calculated using the following formula:

$$R_{AD(0)} = k_2 A^2_{AD(e)}. \tag{5}$$

Adsorption isotherms were fitted using the Langmuir (6) and Freundlich (7) models:

$$A_{AD(e)} = A_{AD(L)} k_{AD(L)} C_{AD(e)} / (1 + k_{AD(L)} C_{AD(e)}), \quad (6)$$

where $A_{AD(L)}$ is the monolayer adsorption capacity, $k_{AD(L)}$ is the Langmuir constant.

$$A_{AD(e)} = k_{AD(F)} \cdot C_{AD(e)}^{1/n}, \quad (7)$$

where $k_{AD(F)}$ and n are Freundlich constants (Al-Ghouti & Da'ana, 2020).

Additionally, the specific adsorption capacity $A_{AD(S)}$ was calculated as: $A_{AD(S)} = 1{,}000 \cdot A_{AD(L)} / S_{BET}$ (μmol/m^2), which is proportional to the surface concentration of adsorption centres (ACs) on the activated carbon.

Results and Discussion

With increasing contact time with HNO_3 solution at room temperature, long-flame coal exhibited a weight gain, denoted as Δ*m*. This gain reached its maximum after approximately 24 hours, after which it either remained constant or gradually declined. In subsequent experiments, a standard nitric acid oxidation time of 24 hours was adopted for all values of R_{OX}. The weight gain Δ*m* exhibited a pronounced dependence on the R_{OX} ratio (Fig. 1), reaching a maximum value of 16% at R_{OX} = 0.4 mol/mol. The decline beyond this point is attributed to low-temperature combustion of the coal's organic matter as a result of oxidative degradation reactions producing CO and CO_2. Based solely on Δ*m* values, the R_{OX} range of 0.4-1.0 mol/mol is considered suboptimal. Nitric acid dissociates to form the nitronium cation, which acts as an electron acceptor. When interacting with coal polyarenes, it produces cation-radical or cationic fragments within the carbon matrix. This significantly enhances the reactivity of the coal and initiates numerous secondary reactions leading to the formation of oxygen-containing functional groups. The nitronium cation also functions as a nitrating agent, converting polyarenes into nitropolyarenes. Structural changes in coal upon interaction with HNO_3 are illustrated by the IR spectra of the original coal sample *D* and the oxidised sample D_{OX} obtained at R_{OX} = 0.4 mol/mol (Fig. 2).

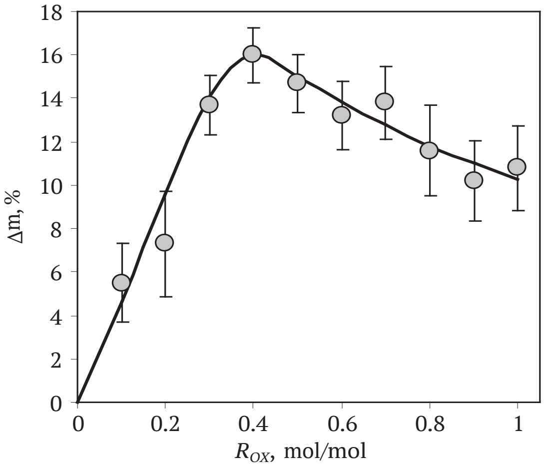

Figure 1. *Weight gain of long-flame coal upon interaction with nitric acid*
Source: *compiled by the authors based on experimental data*

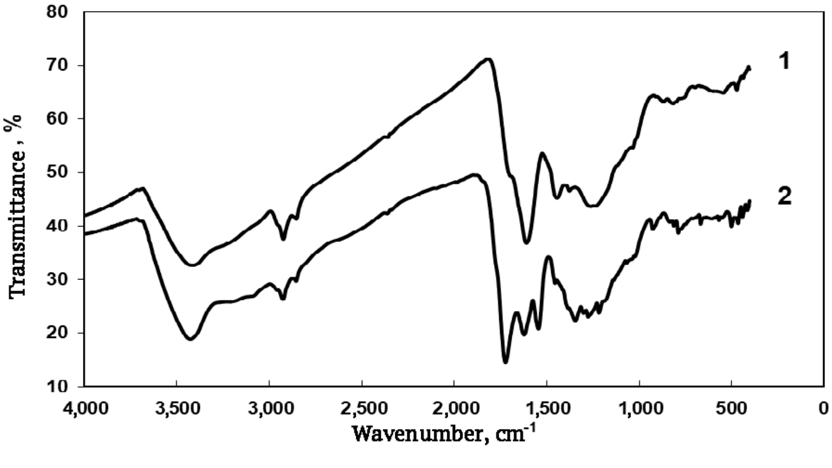

Figure 2. *IR spectra of coal D and oxidised coal* D_{OX}
Note: *1 – coal D, 2 – oxidised coal* D_{OX}
Source: *compiled by the authors based on experimental data*

Both samples contain aromatic fragments, identified by the absorption band corresponding to skeletal vibrations of $C_{ar} = C_{ar}$ bonds at 1,618 cm^{-1}. In the spectrum of coal *D*, bands are observed for isolated hydrogen atoms (868 cm^{-1}), two and three adjacent hydrogen atoms (814 cm^{-1}), and four adjacent hydrogen atoms (755-770 cm^{-1}) within the aromatic ring. The corresponding region for oxidised coal D(A) is considerably more complex. Absorption bands appear at 926 cm^{-1} and 668 cm^{-1} with uncertain assignments, along with absorptions of Car-H bond vibrations at 833 cm^{-1} and 811 cm^{-1} (two adjacent hydrogen atoms) and 787 cm^{-1} (three adjacent hydrogen atoms). Vibrations of Car-H bonds in polynuclear nitroarenes (833 cm^{-1}) and deformation vibrations of NO_2 groups (787 cm^{-1}) were identified. The D_{OX} sample contains carbonyl groups, evidenced by bands at 1,718 cm^{-1} (COOH groups) and a shoulder at 1,760-1,780 cm^{-1} (esters and lactones). Chemolysis with nitric acid introduces nitro groups into the coal, identifiable by absorption bands at 1,540 cm^{-1} and 1,342 cm^{-1}. The nature of substituents in coal arenes changes significantly under nitric acid oxidation due to electrophilic aromatic substitution reactions ($ArH \rightarrow Ar\text{-}NO_2$), oxidation of arene fragments ($ArH \rightarrow Ar\text{-}OH$), oxidation of methyl groups ($Ar\text{-}CH_3 \rightarrow Ar\text{-}COOH$), and the formation of ethers and esters. This fully aligns with the conclusions drawn by L. Giraldo *et al.* (2020). Coal samples oxidised at various R_{OX} ratios were converted into ACs under identical alkaline activation conditions. The characteristics of these ACs are presented in Table 1.

Table 1. *Yield and properties of AC(D) and AC(D_{OX}) samples*

Sample	R_{OX}, mol/mol	Y, %	S_{BET} m^2/g	$A_{CP(e)}$ mmol/g	$A_{CP(S)}$ µmol/m^2	$A_{MB(e)}$ mmol/g	$A_{MB(S)}$ µmol/m^2	$A_{Pb(e)}$ mmol/g	$A_{Pb(S)}$ µmol/m^2
AC(D)	0	50.2	1,685	3.66	2.17	0.72	0.43	0.71	0.42
AC(D_{OX})	0.2	43.9	1,888	4.25	2.25	0.83	0.44	0.92	0.49
	0.4	40.4	2,108	4.43	2.10	0.91	0.43	1.02	0.48
	0.6	39.1	2,100	4.43	2.11	0.90	0.43	1.03	0.49
	0.8	37.7	2,216	4.60	2.08	0.97	0.44	1.11	0.50
	1.0	33.8	2,157	4.59	2.13	1.09	0.51	1.12	0.52

Note: *$A_{CP(e)}$, $A_{MB(e)}$, $A_{Pb(e)}$ are the equilibrium adsorption capacities for 4-chlorophenol, methylene blue, and lead cations, respectively; $A_{CP(S)}$, $A_{MB(S)}$, and $A_{Pb(S)}$ are the specific adsorption capacities for the same adsorbates*
Source: *compiled by the authors based on experimental data*

An increase in the R_{OX} ratio results in an almost linear decrease in AC yield (Fig. 3, Line 1), described by the correlation equation $Y = 48.13 - 14.56 \cdot R_{OX}$ ($R_2 = 0.929$). The reduction in yield is accompanied by further development of the AC surface area (Fig. 3, Line 2). The S_{BET} value increases by a factor of 1.44, with approximately 80% of this surface growth occurring within the R_{OX} range ≤0.4 mol/mol.

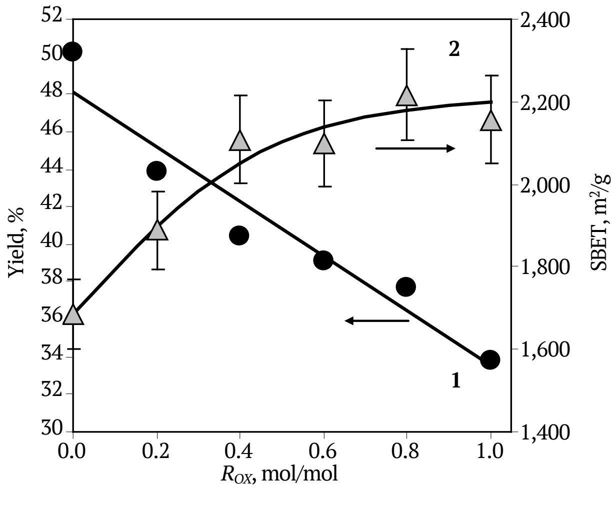

Figure 3. *Yields and specific surface areas (S_{BET}) of AC(D) and AC(D_{OX}) samples* produced at different HNO_3-to-carbon ratios
Note: *1 – yields, 2 – specific surface area (S_{BET})*
Source: *compiled by the authors based on experimental data*

For the AC(D) and AC(D_{OX}) samples, the equilibrium adsorption capacities for CP, MB, and Pb(II) cations from aqueous solutions (25°C, initial adsorbate concentration $C_{AD(0)} = 5$ mmol/L, contact time – 4 hours, AC content – 1 g/L) were measured and are presented in Table 1. With an increase in the R_{OX} ratio, the capacities for CP and Pb(II) increase (Fig. 4), in line with the growth of the specific surface area (S_{BET}). The adsorption capacity for MB also increases and is described by the correlation equation: $A_{MB} = 0.697 - 0.323[HNO_3/C] + 0.742$ ($R^2 = 0.932$), with values ranging from 0.72 to 1.09 mmol/g. The specific adsorption capacity, which reflects the surface concentration of adsorption centres, changes little with increasing R_{OX} ratio (Table 1). The values of $A_{MB(S)}$ and $A_{Pb(S)}$ are similar, ranging from 0.42 to 0.52 µmol/m^2. The values of $A_{CP(S)}$ are 4-5 times higher and remain nearly constant.

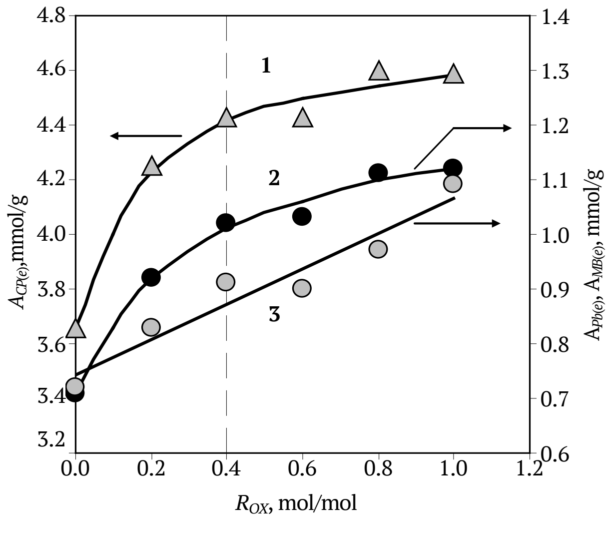

Figure 4. *Adsorption capacities for CP, Pb(II) cations, and MB of AC(D) and AC(D_{ox}) samples produced at different HNO_3-to-carbon ratio*
Note: *1 – adsorption capacity for CP, 2 – adsorption capacity for Pb(II), 3 – adsorption capacity for MB*
Source: *compiled by the authors based on experimental data*

The data obtained showed that nitric acid pre-oxidation of the carbon significantly influences the yield, specific surface area, and adsorption properties of the AC. The primary effect is observed at R_{OX} ratios ⩽ 0.4 mol/mol and manifests in increases in the S_{BET} value (from 1,685 m^2/g to 2,108 m^2/g) and the adsorption capacities for A_{CP} (from 3.66 mmol/g to 4.59 mmol/g), A_{MB} (from 0.72 mmol/g to 1.09 mmol/g), and A_{Pb} (from 0.71 mmol/g to 1.12 mmol/g). However, oxidation has virtually no effect on the surface concentration of ACs. Owing to the marked positive effect of nitric acid oxidation, it was considered appropriate to carry out a more detailed comparison of the properties of two AC samples, namely AC(D) derived from the raw carbon, and AC(D_{OX}), obtained at an R_{OX} ratio of 0.4 mol/mol. The nitrogen adsorption-desorption isotherms at low temperature for these two ACs are shown in Figure 5. At low relative pressures (p/p_0), a sharp increase in the amount of adsorbed nitrogen is observed, which in itself indicates the dominance of microporosity. According to the IUPAC classification (Thommes *et al.,* 2015), these isotherms correspond to type II with H4-type hysteresis, which arises due to the presence of narrow slit-shaped pores and capillary condensation within mesopores.

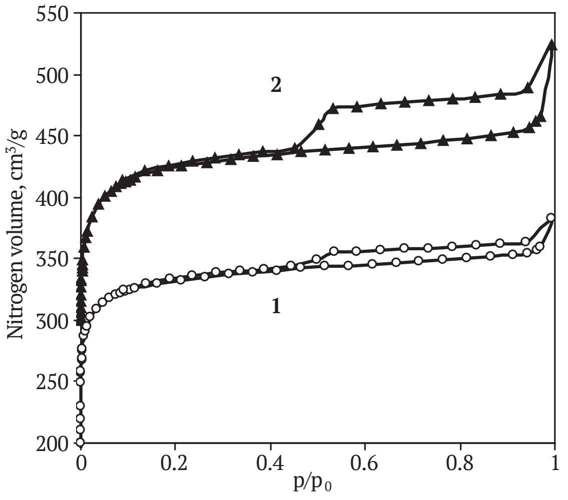

Figure 5. *Nitrogen adsorption-desorption isotherms for AC(D) and AC(D_{OX}) samples*

Note: *1 – sample AC(D), 2 – sample AC(D_{OX})*

Source: *compiled by the authors based on experimental data*

Integral pore volume versus average pore diameter (*D*) relationships, calculated using the 2D-NLDFT method (Fig. 6), showed the following. Alkaline activation primarily produces microporosity, with the majority of the total pore volume attributed to pores with $D \leqslant 5$ nm. Both samples lack pores with diameters in the range D = 5-15 nm, but contain mesopores with $D \geqslant 15$ nm. A comparison of the V_t vs D relationships and pore size distributions (Fig. 7) indicates that nitric acid oxidation primarily promotes the additional formation of micropores and mesopores with diameters of D = 2-5 nm, while having virtually no effect on the development of pores of other sizes. The S_{DFT} vs D dependencies exhibit similar trends.

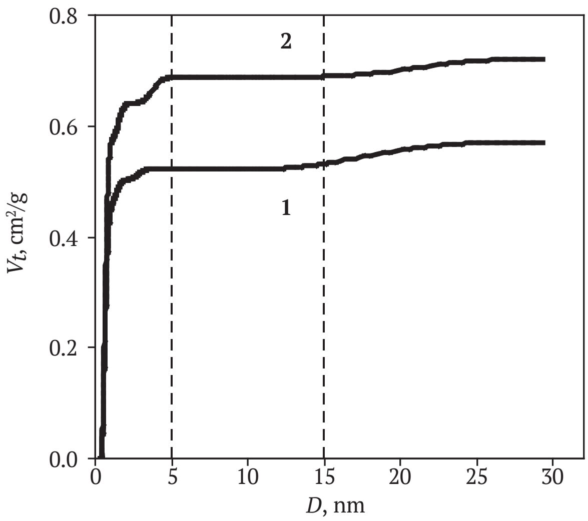

Figure 6. *Integral pore volume as a function of pore diameter for AC(D) and AC(D_{OX}) samples*

Note: *1 – sample AC(D), 2 – sample AC(D_{OX})*

Source: *compiled by the authors based on experimental data*

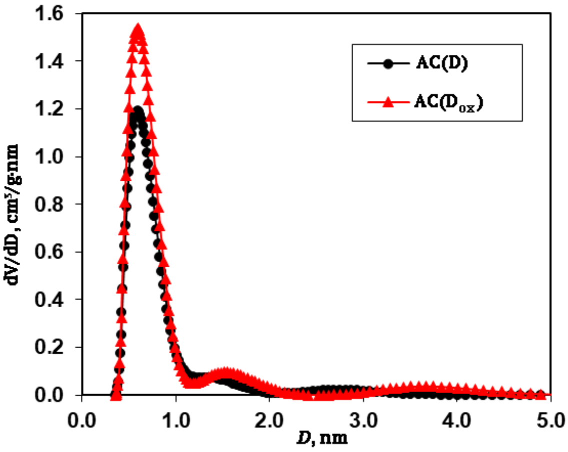

Figure 7. *Pore size distribution of AC(D) and AC(D_{OX}) samples*

Source: *compiled by the authors based on experimental data*

A comparison of the pore volumes and specific surface areas of various pore types in the two AC samples (Table 2) reveals the following. Preliminary nitric acid oxidation results in a 37% increase in total pore volume, a 29% increase in ultramicropore volume, a 27% increase in supermicropore and subnanopore volumes, and a 28% increase in micropore volume. The most substantial increase (88%) is observed in the combined volume of meso- and macropores. The specific surface area S_{DFT} increases by 27%, and S_{me+ma} increases by 50%. The specific surface areas of the other pore types grow proportionally with their volume increases.

Table 2. *Pore volumes and specific surface areas of various pores in AC(D) and AC(D_{OX}) samples*

Sample	Pore volume, cm³/g					
	V_t	V_{umi}	V_{smi}	V_{1nm}	V_{mi}	V_{me+ma}
AC(D)	0.59	0.28	0.22	0.44	0.50	0.09
AC(D_{OX})	0.81	0.36	0.28	0.56	0.64	0.17
Sample	**Specific surface area, m²/g**					
	S_{DFT}	S_{umi}	S_{umi}	S_{1nm}	S_{mi}	S_{me+ma}
AC(D)	1,510	980	510	1,400	1,490	20
AC(D_{OX})	1,920	1,270	620	1,780	1,890	30

Note: *explanations of the designations used for pore volume and specific surface area are provided in the Materials and Methods section*

Source: *compiled by the authors based on experimental data*

Oxidation reduces the proportion of micropore volume ($P_{V(mi)}$) due to an increase in the proportion of meso- and macropores (Table 3). This effect is most pronounced in the subnanopore volume fraction ($P_{V(1nm)}$). However, the proportion of specific surface area attributed to these pores ($P_{S(1nm)}$) remains largely unchanged. Both samples exhibit a high proportion of micropore surface area, amounting to no less than 98%. This indicates that the resulting ACs can be classified as microporous materials, with a predominance of ultramicroporosity.

Table 3. *Pore volumes and specific surface area fractions of various pore types in AC(D) and AC(D_{OX}) samples*

Sample	Pore volume fractions, %				
	$P_{V(umi)}$	$P_{V(smi)}$	$P_{V(1nm)}$	$P_{V(mi)}$	$P_{V(me+ma)}$
AC(D)	47	37	75	85	15
AC(D_{OX})	44	35	69	79	21
Sample	**Specific surface area fractions, %**				
	$P_{S(umi)}$	$P_{S(smi)}$	$P_{S(1nm)}$	$P_{S(mi)}$	$P_{S(me+ma)}$
AC(D)	65	34	93	99	1
AC(D_{OX})	66	32	93	98	2

Note: *explanations of the designations used for pore volume and specific surface area are provided in the Materials and Methods section*

Source: *compiled by the authors based on experimental data*

The adsorption kinetics of CP, MB, and Pb(II) cations were measured at an identical initial concentration of $C_{AD(0)} = 5$ mmol/L. Adsorption equilibrium was reached within 2-4 hours, depending on the nature of the adsorbate, as illustrated in Figure 8 for the AC(D_{OX}) sample.

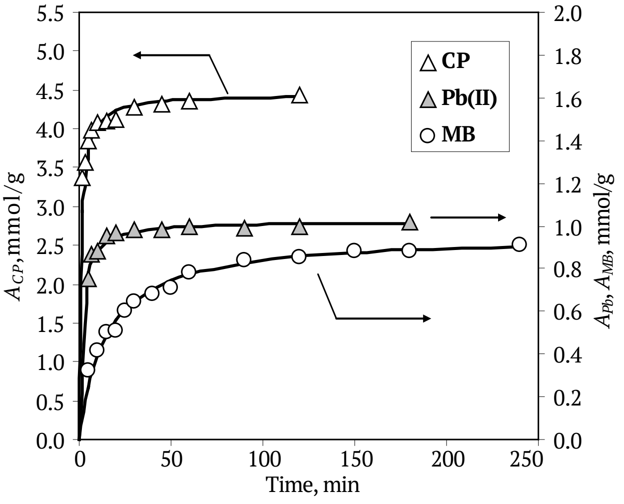

Figure 8. *Adsorption kinetics for the AC(D_{OX}) sample*

Source: *compiled by the authors based on experimental data*

Kinetic curves of a similar shape were also observed for the AC(D) sample. The kinetic model parameters are presented in Table 4. The adsorption kinetics of CP and Pb(II) are poorly approximated by the pseudo-first-order model ($R^2 \leqslant 0.912$), whereas this model is more suitable for the adsorption of MB ($R^2 \geqslant 0.963$). A better fit for describing the kinetics is provided by the pseudo-second-order model, which was used to calculate the solid lines shown in Figure 8. This model suggests that the rate of adsorption is limited by the interaction between the adsorbate and the AC surface (Revellame *et al.*, 2020), rather than by diffusion into the porous structure of the AC. The highest adsorption capacities were observed for CP. The values of $A_{AD(e)}$ differ by a factor of 4.4 to 5.2 depending on the adsorbate, while the k_2 values vary by a factor of 6.1 for AC(D) and 8.8 for AC(D_{OX}). The highest initial adsorption rate is recorded for CP, and the lowest for MB. The differences in $R_{AD(0)}$ rate between the adsorbates are substantial – up to 105-fold for AC(D) and 65-fold for AC(D_{OX}). Oxidation with nitric acid promotes the formation of ACs with enhanced adsorption rates – 1.2 times faster for CP, 1.9 times for MB, and 4.1 times for Pb(II) cations. This indicates a significant improvement in the efficiency of ACs for rapid water purification applications. The amount of adsorbate taken up during the initial stage of adsorption can be estimated using the adsorption capacity $A_{AD(1)}$, calculated for the first minute of the process. Accordingly, the ratio $A_{AD(1)}/A_{AD(e)}$ reflects the efficiency of adsorbate uptake by the AC samples during the early phase. Data from Table 4 show that the lowest efficiency is observed during the adsorption of MB (0.65%-1.24%), while the highest is recorded for CP: approximately half of the maximum amount of 4-chlorophenol is adsorbed within the first minute. This property of the adsorbent is particularly important for the rapid removal of highly toxic compounds from water. The kinetic data were additionally approximated using the intraparticle diffusion model, as illustrated for the AC(D_{OX}) sample in Figure 9.

***Table 4.** Parameters of kinetic models of adsorption by samples AC(D) and AC(D_{OX})*

Sample	Model	Parameter	Adsorbate		
			CP	MB	Pb(II)
AC(D)	Pseudo-first-order	$A_{AD(exp)}$, mmol/g	3.66	0.72	0.71
		$k_1 \cdot 10^2$, min^{-1}	7.65	2.42	0.25
		R^2	0.824	0.985	0.715
	Pseudo-second-order	$A_{AD(e)}$, mmol/g	3.70	0.82	0.72
		k_2, g/mmol·min	0.26	0.051	0.31
		$R_{AD(0)}$, mmol/g·min	3.56	0.034	0.16
		$A_{AD(1)}$, mmol/g	1.81	0.033	0.13
		$A_{AD(1)}/A_{AD(e)}$, %	36	0.65	2.6
		R^2	0.998	0.997	0.998
AC(D_{OX})	Pseudo-first-order	$A_{AD(exp)}$, mmol/g	4.43	0.91	1.02
		$k_1 \cdot 10^2$, min^{-1}	4.18	1.83	1.84
		R^2	0.912	0.963	0.651
	Pseudo-second-order	$A_{AD(e)}$, mmol/g	4.45	0.96	1.03
		k_2, g/mmol·min	0.22	0.072	0.63
		$R_{AD(0)}$, mmol/g·min	4.29	0.066	0.65
		$A_{AD(1)}$, mmol/g	2.19	0.062	0.40
		$A_{AD(1)}/A_{AD(e)}$, %	44	1.24	8.0
		R^2	0.997	0.998	0.998

***Note:** explanations of the designations used for adsorption kinetic parameters are provided in the Materials and Methods section*
***Source:** compiled by the authors based on experimental data*

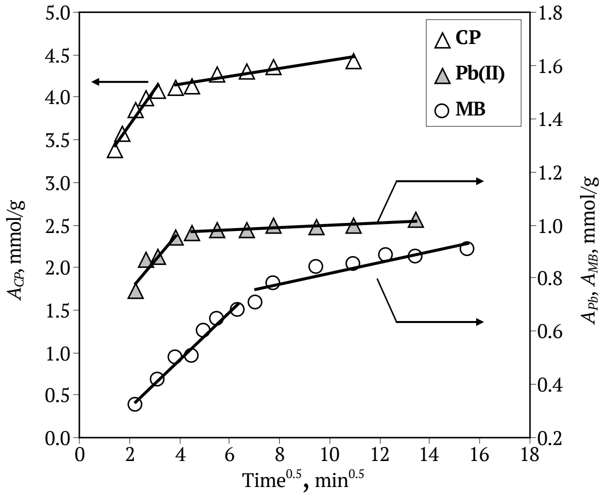

***Figure 9.** Application of the intraparticle diffusion model to adsorption by AC(D_{OX}) sample*
***Source:** compiled by the authors based on experimental data*

A similar pattern was observed for AC(D_{OX}), and the coefficients of the equations are presented in Table 5. This model implies the following: 1) the presence of several linear segments indicates that multiple adsorption mechanisms are involved; 2) diffusion is the rate-limiting step if the dependence of A_{AD} versus $\tau^{0.5}$ passes through the origin ($C_{d1} = 0$) (Wang & Guo, 2022). For both AC samples, the A_{AD} versus $\tau^{0.5}$ dependencies exhibit two linear regions, indicating the involvement of at least two adsorption mechanisms. This is observed for all adsorbates, albeit within different time intervals. For CP adsorption, the first mechanism dominates during the initial ~10 minutes; for Pb(II) cations, during 15-20 minutes; and for MB, during 40-50 minutes. The adsorption of MB by AC(D) sample is characterised by a low C_{d1} value (–0.05 mmol/g), suggesting that the rate of adsorption is limited by diffusion. Additionally, MB molecules are significantly larger than the other adsorbates, which hinders their transport into the microporous structure of AC. However, this limitation is mitigated in the case of AC derived from oxidised coal. In the remaining cases, the initial segments do not pass through the origin ($C_{d1} > 0$), indicating the absence of diffusion constraints during the early stage of adsorption. This finding is consistent with the better applicability of the pseudo-second-order model, which also assumes no diffusion limitation. The adsorption isotherms for AC(D) and AC(D_{OX}) samples are presented in Figures 10 and 11, respectively. The data were approximated using the Langmuir and Freundlich models, which are the most commonly applied to describe the adsorption of the selected adsorbates from aqueous media.

***Table 5.** Parameters of the intraparticle diffusion model for adsorption by AC(D) and AC(DOX) samples*

Sample	Adsorbate	Parameters					
		k_{d1}, mmol/g·min$^{0.5}$	kd2, mmol/g·min$^{0.5}$	C_{d1}, mmol/g	C_{d2}, mmol/g	R^2_{d1}	R^2_{d2}
AC(D)	CP	0.535	0.017	1.660	3.497	0.937	0.526
	MB	0.091	0.015	–0.05	0.506	0.964	0.865
	Pb(II)	0.060	0.011	0.322	0.571	0.950	0.994
AC(D_{OX})	CP	0.410	0.046	2.854	3.965	0.956	0.871
	MB	0.091	0.021	0.130	0.606	0.975	0.840
	Pb(II)	0.109	0.005	0.539	0.951	0.854	0.859

***Note:** k_{d1} and k_{d2} are the rate constants of the intraparticle diffusion model for the first and second linear regions shown in Figure 9; C_{d1} and C_{d2} are the intercepts; R^2_{d1} and R^2_{d2} are the determination coefficients for the approximations of the first and second regions*
***Source:** compiled by the authors based on experimental data*

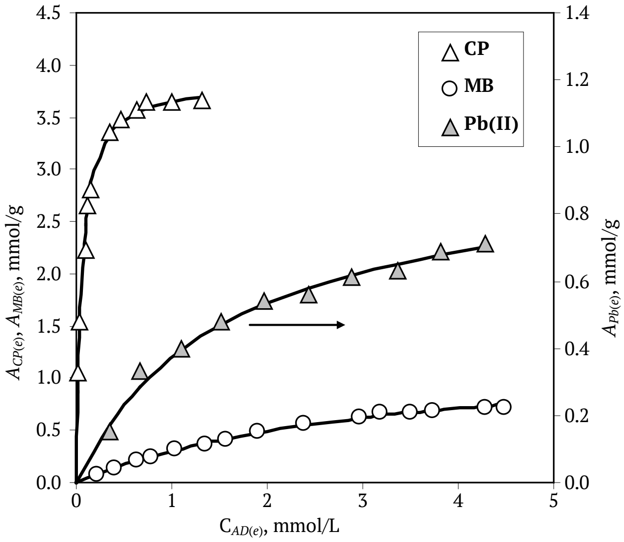

***Figure 10.** Adsorption isotherms for the AC(D) sample*
***Source:** compiled by the authors based on experimental data*

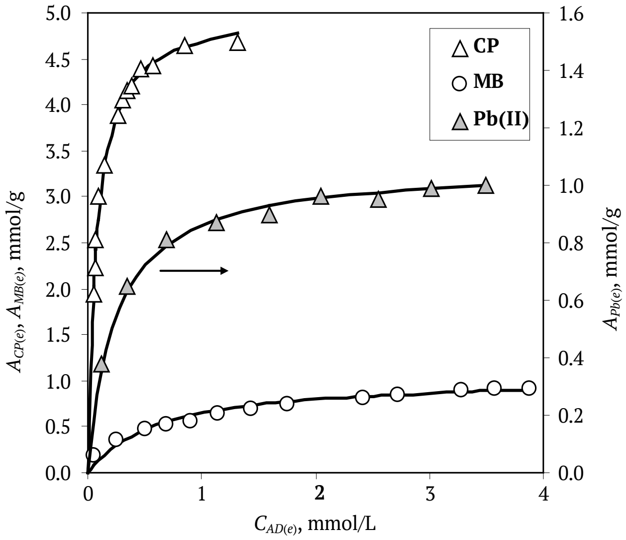

***Figure 11.** Adsorption isotherms for the AC(D_{OX}) sample*
***Source:** compiled by the authors based on experimental data*

From the linearised forms of these models, the parameters of the Langmuir (using the coordinates “$C_{AD(e)}/A_{AD(e)}$) – $C_{AD(e")}$ and Freundlich (using “$lnA_{AD(e)}$) – $lnC_{AD(e)}$”) equations were calculated, and the results are presented in Table 6. The Langmuir model assumes a chemically homogeneous surface of the AC and that the maximum adsorption capacity corresponds to a saturated monolayer of adsorbate, denoted as $A_{AD(L)}$. In contrast, the Freundlich model describes multilayer adsorption on a chemically heterogeneous surface containing adsorption sites with varying activity. The *1/n* coefficient accounts for surface heterogeneity, reflected in the range of interaction energies between ACs and adsorbate molecules. Adsorption is considered favourable when 0 < *1/n* < 1, while values of *1/n* > 1 indicate an unfavourable process (Al-Ghouti & Da’ana, 2020).

***Table 6.** Adsorption isotherm parameters for the AC(D) and AC(D_{OX}) samples*

Sample	Model	Parameter	Adsorbate		
			CP	MB	Pb(II)
AC(D)	Langmuir	$A_{AD(L)}$, mmol/g	3.834	1.282	0.960
		$k_{AD(L)}$, L/mmol	19.38	0.311	0.622
		$A_{AD(S)}$, µmol/m^2	2.54	0.85	0.64
		R^2	0.998	0.991	0.984
	Freundlich	$k_{AD(F)}$, (mmol/g)(L/mmol)$^{1/n}$	4.042	0.282	0.343
		1/n	0.276	0.734	0.556
		R^2	0.915	0.987	0.931

Table 6. Continued

Sample	Model	Parameter	Adsorbate		
			CP	**MB**	**Pb(II)**
AC(D_{OX})	Langmuir	$A_{AD(L)}$, mmol/g	5.043	1.037	1.069
		$k_{AD(L)}$, L/mmol	13.398	1.674	4.097
		$A_{AD(S)}$, μmol/m^2	2.63	0.54	0.56
		R^2	0.998	0.992	0.998
	Freundlich	$k_{AD(F)}$, (mmol/g)(L/mmol)$^{1/n}$	5.788	0.582	0.774
		$1/n$	0.325	0.365	0.256
		R^2	0.936	0.991	0.904

Source: *compiled by the authors based on experimental data*

According to the determination coefficients, the Langmuir model provides a better fit to the isotherm data. The values of the saturated monolayer capacity $A_{AD(L)}$ differ by a factor of 4.0-4.9 across the adsorbates and, for the AC(D) sample, increase in the order: Pb(II) < MB < CP. For the AC(D_{OX}) sample, the sequence differs: MB < Pb(II) < CP, although the $A_{AD(L)}$ values for Pb(II) and MB are nearly identical. The numerical values of $A_{AD(L)}$ (Table 6) are within the commonly reported range. According to the literature, the adsorption capacity of most ACs for CP generally ranges from 0.33 to 2.52 mmol/g (Chen *et al.*, 2017), and for Pb(II) cations from 0.029 to 1.42 mmol/g (Ghorbani *et al.*, 2020). The capacity for MB typically varies between 0.021 and 2.58 mmol/g (Oladoye *et al.*, 2022; Jasri *et al.*, 2023), although significantly higher values of $A_{MB(L)}$ = 5.50-7.04 mmol/g have also been reported (Li *et al.*, 2021). Comparison of the obtained results with published data indicates that both AC(D) and AC(D_{OX}) samples exhibit acceptable capacities for MB and Pb(II) cations, as well as high adsorption capacities for 4-chlorophenol. The adsorption constants $k_{AD(L)}$ for AC(D) vary by a factor of 62 across the different adsorbates, whereas for AC(D_{OX}) the variation is only eightfold. This suggests that preoxidation of the coal makes the AC significantly less sensitive to the adsorbate's nature, thereby reducing adsorption selectivity.

A comparison of the adsorption parameters for the two AC samples yields the following observations. The AC(D_{OX}) sample adsorbs greater quantities of all adsorbates (Table 4): 1.20 times more CP, 1.17 times more MB, and 1.43 times more Pb(II) cations. For Pb(II) and MB, the specific adsorption capacities $A_{AD(S)}$ of AC(D_{OX}) are lower than those of AC(D), while for CP, the $A_{AD(S)}$ value is higher, although not substantially so. The lower surface concentrations of adsorbed Pb(II) and MB suggest that treatment with HNO_3 negatively affects the formation of ACs under alkaline activation conditions. The AC(D) and AC(D_{OX}) samples exhibit significantly higher surface concentrations of ACs – 4 to 5 times greater – that are active exclusively towards CP. This may be attributed to structural features, including differences in the number of functional groups and the presence of graphene fragments within the spatial framework of the AC. The initial adsorption rate of CP is high for both materials (Table 4), although it is 1.2 times higher for the AC(D_{OX}) sample. Other adsorbates are also absorbed more rapidly by this sample: MB at twice the rate, and Pb(II) cations at four times the rate. Furthermore, the oxidised carbon material possesses a more developed total surface area and a subnanoporous structure. Consequently, the AC(D_{OX}) sample is a more effective adsorbent than the AC(D) material derived from unoxidised long-flame coal.

Overall, nitric acid oxidation has a pronounced impact on the properties of AC. In the study by Y. Gokce & Z. Aktas (2014), it was demonstrated that treating AC with an HNO_3 solution at 90°C damages the porous structure. As the concentration of nitric acid increases to 80%, the pore volume decreases from 1.18 cm^3/g to 0.02 cm^3/g, while the specific surface area decreases from 1,398 m^2/g to 49 m^2/g. This substantial reduction in S_{BET} (by a factor of 28.5) and V_t (by a factor of 59) was attributed to the destruction of pore walls due to oxidative degradation, which transforms micro- and mesopores into macropores.in the process. These trends are qualitatively supported by the findings of I. Demiral *et al.* (2021) investigated the oxidation of AC with nitric acid (⩽ 69%) under similar conditions (90°C). Increasing the HNO_3 concentration to 69% led to a 16.1-fold reduction in V_t (from 0.680 cm^3/g to 0.042 cm^3/g) and a 93.3-fold decrease in S_{BET} (from 1,399 m^2/g to 15 m^2/g). According to W. Somyanonthanakun *et al.* (2023), oxidation of biomass-derived AC under milder conditions (4 hours, 80°C, $[HNO_3]$ = 4-10 M) resulted in less severe degradation of the porous structure, with S_{BET} decreasing by a factor of 1.8 (from 767 m^2/g to 418 m^2/g) and V_t by a factor of 3.7 (from 0.78 cm^3/g to 0.21 cm^3/g). A deterioration of pore structure parameters – typically by factors of 2 to 6 – as a result of nitric acid oxidation was also reported by L. Giraldo *et al.* (2020) for lignocellulosic-based AC, by E. Wolak & A. Orzechowska-Zięba (2024) for industrial AC, and by L.S. Queiroz *et al.* (2020) for a series of ACs prepared via alkaline activation of biomass with various KOH ratios (R_{KOH} = 1-5 g/g). Analysis of the aforementioned studies indicates that pore structure degradation occurs in all cases. However, the extent of this degradation depends both on the oxidation conditions and the type of AC used, with no clear patterns identified to date.

A more complex picture emerges when oxidation with nitric acid is carried out at room temperature. According to H.-K. Kim *et al.* (2024), treating AC at 25 °C for 24 hours in solutions with HNO_3 concentrations ⩽3 M reduced the specific surface area from 1,027 m^2/g to 746 m^2/g, whereas a concentration of 5 M resulted in an increase to 793 m^2/g.

This effect was attributed to oxidative destruction that opens previously closed internal pores of AC – an effect not observed in the studies by Y. Gokce & Z. Aktas (2014), I. Demiral *et al.* (2021), or W. Somyanonthanakun *et al.* (2023). An opposite trend was reported by X. Jiang *et al.* (2019) for coke-derived AC under similar oxidation conditions (25°C, 4 hours): increasing the HNO_3 concentration to 3 M increased the S_{BET} from 642 m^2/g to 802 m^2/g, but further increasing it to 4 M reduced it to 689 m^2/g. Overall, the negative effect of oxidation on AC porosity is mitigated at lower HNO_3 concentrations and lower temperatures, though the outcome varies depending on the carbon precursor material. An unusual effect was first identified in a study by R. Pietrzak *et al.* (2009): while nitric acid oxidation of AC reduced the specific surface area from 2,876 m^2/g to 359 m^2/g – consistent with other studies – oxidising the precursor material (orthocoke fossil coal) increased the surface area to 3,087 m^2/g. This effect was confirmed by data from J.H. Kim *et al.* (2019) for wood-derived AC: contact with an HNO_3 solution (5%, 80°C, 12 hours) reduced the S_{BET} from 1,485 m^2/g to 833 m^2/g, while subsequent alkaline activation increased it to 2,027 m^2/g. A similar trend is observed in the present study when oxidising the precursor – long-flame coal (Table 1).

Nitric acid oxidation also affects the adsorption properties of AC, although systematic data remain limited. Y. Gokce & Z. Aktas (2014) found that AC oxidation increased the adsorption capacity for MB by a factor of 1.6 – from 1.34 mmol/g to 2.14 mmol/g – despite a substantial 28.5-fold reduction in specific surface area. This indicates an increase in the surface concentration of the adsorbed dye from 0.75 $\mu mol/m^2$ to 2.55 $\mu mol/m^2$. An even greater increase in MB capacity was reported by D.H. Nguyen *et al.* (2019) following nitric acid oxidation of biomass carbonisate: the $A_{MB(L)}$ value increased 4.5-fold (from 0.17 mmol/g to 0.77 mmol/g), while the specific surface area changed only slightly (decreasing from 7.33 m^2/g to 4.49 m^2/g). Of particular note is that oxidation significantly improved the adsorption performance of a carbon material with a poorly developed surface (S_{BET} = 4.49 m^2/g), corresponding to a specific capacity of $A_{MB(S)}$ = 170 $\mu mol/m^2$. In the present study, oxidation also increases the $A_{MB(e)}$ value, although the specific capacity changes only slightly and remains within the range $A_{MB(S)}$ = 0.430.51 $\mu mol/m^2$ (Table 1). A comparison of the MB adsorption data suggests that oxidation of the precursor affects the adsorption properties of AC differently from the oxidation of the AC itself. The iodine adsorption capacity varies in parallel with changes in specific surface area following nitric acid oxidation, as reported by R. Pietrzak *et al.* (2009) and X. Jiang *et al.* (2019). However, a strict proportionality between the I2 capacity and S_{BET} is not maintained.

The most pronounced effect of HNO_3 treatment is the enhancement of the adsorption activity of AC with respect to lead cations. This is attributed to the increased content of hydroxyl and acidic functional groups in oxidised carbon materials (Rudenko *et al.*, 2021). For instance, according to W. Somyanonthanakun *et al.* (2023), AC oxidation increases the Pb(II) adsorption capacity 3.5-fold (from 0.29 mmol/g to 1.02 mmol/g), even though the specific surface area decreases from 767 cm^2/g to 418 cm^2/g. The adsorption kinetics are better described by the pseudo-second-order equation, and the adsorption isotherms fit the Langmuir model, which aligns with the present study's findings (Tables 4 and 6). The $k_{Pb(L)}$ values range from 6.22 to 103 L/mol, and k_2 values fall within 1.24-9.53 g/mmol·min, showing little dependence on HNO_3 concentration. In this case, the rate constants are significantly lower, although the Pb(II) adsorption capacities are of the same order of magnitude.

Analysis of the presented data reveals fundamentally different outcomes of nitric acid oxidation applied to the precursor and the resulting activated carbon. Oxidation of AC reduces its specific surface area and pore volume, transforms its microporous structure into a macroporous one, and partially destroys the carbon spatial framework. In contrast, oxidation of the precursor enhances its chemical reactivity during activation, increases the specific surface area of the resulting AC, and promotes micropore formation. Nitric acid oxidation of the precursor is thus an independent and equally important method of influencing the porous structure and adsorption properties of activated carbon.

Conclusions

For the first time, the porous structure and properties of AC samples derived from long-flame coal through a combination of nitric acid oxidation and alkaline activation at a low KOH-to-coal ratio (1 g/g) have been investigated. Interaction with a 50% HNO_3 solution immobilises structural oxygen and nitrogen within the coal via the formation of phenolic, carboxylic and nitro groups, as well as ethers and esters. This is accompanied by an increase in coal mass, which exhibits a pronounced dependence on the HNO_3-to-carbon ratio in the range R_{OX} = 0.1-1.0 mol/mol, with a maximum increase (16%) observed at R_{OX} = 0.4 mol/mol. Coal samples oxidised at various R_{OX} ratios were converted into AC under identical alkaline activation conditions. It was found that increasing the R_{OX} ratio from 0 to 1.0 mol/mol reduces the AC yield (from 50.2% to 33.85%) but increases the specific surface area (from 1,685 m^2/g to 2,216 m^2/g). The dominant portion (~80%) of the effect occurs within the range of $R_{OX} \leqslant 0.4$ mol/mol. The adsorption capacities of the AC for 4-chlorophenol (CP), methylene blue (MB), and Pb(II) cations also increase with rising R_{OX}. The obtained results demonstrate that preliminary nitric acid oxidation of coal has a significant effect on the yield, specific surface area, and adsorption properties of the AC. The most pronounced influence is observed at $R_{OX} \leqslant 0.4$ mol/mol. A detailed comparison was made between two samples: AC(D), derived from untreated coal, and AC(D_{OX}), obtained from coal oxidised at R_{OX} = 0.4 mol/mol. The nitrogen adsorption–desorption isotherms at low temperature correspond to type II with an H4-type hysteresis loop, according to the IUPAC classification. Analysis of the pore volume and surface area as a function of pore diameter (*D*) revealed that nitric acid oxidation most significantly promotes the additional formation of micropores and mesopores with D = 2-5 nm, while it has little effect on the development of pores of other sizes. Both samples exhibit a high proportion (98%) of micropore surface area, indicating that the AC is microporous in nature, with a predominance of ultramicroporosity.

Kinetic measurements of CP, MB, and Pb(II) adsorption showed that equilibrium is reached within 2-4 hours, depending on the nature of the adsorbate. The kinetic curves are better described by the pseudo-second-order model, suggesting that the adsorption rate is limited by interactions between the adsorbate and surface active sites of the AC. This is further supported by the application of the intraparticle diffusion model. The adsorption isotherms are best fitted by the Langmuir model, from which the monolayer adsorption capacities of the adsorbates were calculated. Comparison with published data indicates that both AC(D) and AC(D_{OX}) possess acceptable adsorption capacities for MB and Pb(II) and exhibit high adsorption capacities for CP. The Langmuir constants for AC(D) vary by a factor of 62 across different adsorbates, whereas for AC(D_{OX}), the variation is only by a factor of 8. This suggests that pre-oxidation of oxidised coal renders the AC significantly less sensitive to the nature of the adsorbate and reduces adsorption selectivity. Compared to AC(D), the AC(D_{OX}) sample adsorbs greater quantities of CP (1.20 times more), MB (1.17 times more), and Pb(II) cations (1.43 times more). The initial adsorption rate of CP is high for both materials, but it is 1.2 times faster for AC(D_{OX}). Other adsorbates are also absorbed more rapidly by this sample: MB at twice the rate, and Pb(II) cations at four times the rate. This property is particularly important for the rapid removal of highly toxic compounds from water. Furthermore, the oxidised coal-based material exhibits a more developed overall surface area and a subnanoporous structure. Therefore, AC(D_{OX}) sample is a more effective adsorbent than AC(D), which is derived from non-oxidised long-flame coal. The results obtained provide a positive assessment of the effect of nitric acid oxidation of coal on the adsorption properties of AC produced via alkaline activation. Future research will focus on determining the impact of oxidation on the characteristics of AC derived from highly metamorphosed coals, particularly anthracites, which exhibit low chemical reactivity towards alkalis. Additional studies will also explore further practical applications of the AC, including its use in radionuclide and toxic compound capture and energy storage for supercapacitors.

Acknowledgements

The authors would appreciate to thank Dr. R.D. Mysyk (Basque Research and Technology Alliance, Spain) for his assistance in conducting adsorption measurements and calculations of low-temperature nitrogen adsorption isotherms.

Funding

Financial support for this work was provided by the National Academy of Sciences of Ukraine (State Registration Number: 0117U000022).

Conflict of Interest

None.

References

[1] Al-Ghouti, M.A., & Da'ana, D.A. (2020). Guidelines for the use and interpretation of adsorption isotherm models: A review. *Journal of Hazardous Materials*, 393, article number 122383. doi: 10.1016/j.jhazmat.2020.122383.

[2] Bellamy, L.J. (1975). *The infra-red spectra of complex molecules*. Dordrecht: Springer Dordrecht. doi: 10.1007/978-94-011-6017-9.

[3] Bergna, D., Varila, T., Romar, H., & Lassi, U. (2022). Activated carbon from hydrolysis lignin: Effect of activation method on carbon properties. *Biomass and Bioenergy*, 159, article number 106387. doi: 10.1016/j.biombioe.2022.106387.

[4] Chen, C., Geng, X., & Huang, W.A. (2017). Adsorption of 4-chlorophenol and aniline by nanosized activated carbons. *Chemical Engineering Journal*, 327, 941-952. doi: 10.1016/j.cej.2017.06.183.

[5] Demiral, I., Samdan, C., & Demiral, H. (2021). Enrichment of the surface functional groups of activated carbon by modification method. *Surfaces and Interfaces*, 22, article number 100873. doi: 10.1016/j.surfin.2020.100873.

[6] DSTU 3472-96. (2009). *Lignite, hard coal and anthracite. Classification. With Amendment (IPS No. 9-2003) and Amendment No. 1 (IPS No. 12-2009)*. Retrieved from https://online.budstandart.com/ua/catalog/doc-page.html?id_doc=29353.

[7] Ghorbani, M., Seyedin, O., & Aghamohammadhassan, M. (2020). Adsorptive removal of lead (II) ion from water and wastewater media using carbon-based nanomaterials as unique sorbents: A review. *Journal of Environmental Management*, 254, article number 109814. doi: 10.1016/j.jenvman.2019.109814.

[8] Giraldo, L., Vargas, D.P., & Moreno-Piraján, J.C. (2020). Study of CO_2 adsorption on chemically modified activated carbon with nitric acid and ammonium aqueous. *Frontiers in Chemistry*, 8, article number 543452. doi: 10.3389/fchem.2020.543452.

[9] Gokce, Y., & Aktas, Z. (2014). Nitric acid modification of activated carbon produced from waste tea and adsorption of methylene blue and phenol. *Applied Surface Science*, 313, 352-359. doi: 10.1016/j.apsusc.2014.05.214.

[10] Jagiello, J., Kyotani, T., & Nishihara, H. (2020). Development of a simple NLDFT model for the analysis of adsorption isotherms on zeolite templated carbon (ZTC). *Carbon*, 169, 205-213. doi: 10.1016/j.carbon.2020.06.032.

[11] Jiang, X., Lan, X., Song, Y., & Xing, X. (2019). Adsorption of COD in coking wastewater on nitric acid-modified blue coke activated carbon. *Journal of Chemistry*, 2019(1), article number 8593742. doi: 10.1155/2019/8593742.

[12] Kim, H.-K., Kim, S.-J., Kim, H.-R., & Park, J.-W. (2024). Nitric acid modified powdered activated carbon for simultaneous adsorption of lead and phenol in aqueous solution. *Journal of Environmental Chemical Engineering*, 12(6), article number 114889. doi: 10.1016/j.jece.2024.114889.

[13] Kim, J.H., Hwang, S.Y., Park, J.E., Lee, G.B., Kim, H., Kim, S., & Hong, B.U. (2019). Impact of the oxygen functional group of nitric acid-treated activated carbon on KOH activation reaction. *Carbon Letters*, 29, 281-287. doi: 10.1007/s42823-019-00024-0.

[14] Lee, S.-Yi., & Mahajan, R.L. (2021). A facile method for coal to graphene oxide and its application to a biosensor. *Carbon*, 181, 408-420. doi: 10.1016/j.carbon.2021.05.007.

[15] Lee, S.M., Lee, S.H., Park, S., Yoon, S.-H., & Jung, D.-H. (2022). Preparation of mesoporous activated carbon by preliminary oxidation of petroleum coke with hydrogen peroxide and its application in capacitive deionization. *Desalination*, 539, article number 115901. doi: 10.1016/j.desal.2022.115901.

[16] Li, L., Wu, M., Song, C., Liu, L., Gong, W., Ding, Y., & Yao, J. (2021). Efficient removal of cationic dyes via activated carbon with ultrahigh specific surface derived from vinasse wastes. *Bioresource Technology*, 322, article number 124540. doi: 10.1016/j.biortech.2020.124540.

[17] Li, M., Liu, X., Sun, C., Stevens, L., & Liu, H. (2022). Synthesis and characterization of advanced bio-carbon materials from Kraft lignin with enhanced CO_2 capture properties. *Journal of Environmental Chemical Engineering*, 10(3), article number 107471. doi: 10.1016/j.jece.2022.107471.

[18] Nguyen, D.H., Tran, H.N., Chao, H.-P., & Lin, C.-C. (2019). Effect of nitric acid oxidation on the surface of hydrochars to sorb methylene blue: An adsorption mechanism comparison. *Adsorption Science & Technology*, 37(7-8) 607-622. doi: 10.1177/0263617419867519.

[19] Oladoye, P.O., Ajiboye, T.O., Omotola, E.O., & Oyewola, O.J. (2022). Methylene blue dye: Toxicity and potential elimination technology from wastewater. *Results in Engineering*, 16, article number 100678. doi: 10.1016/j.rineng.2022.100678.

[20] Pietrzak, R., Nowicki, P., & Wachowska, H. (2009). The influence of oxidation with nitric acid on the preparation and properties of active carbon enriched in nitrogen. *Applied Surface Science*, 255(6), 3586-3593. doi: 10.1016/j.apsusc.2008.10.002.

[21] Queiroz, L.S., Souza, L.K.C.D., Thomaz, K.T.C., Lima, E.T.L., Rocha Filho, G.N., Nascimento, L.A.S.D., Oliveira Pires, L.H., Faial, K.D.C.F., & da Costa, C.E.F. (2020). Activated carbon obtained from amazonian biomass tailings (acai seed): Modification, characterization, and use for removal of metal ions from water. *Journal of Environmental Management*, 270, article number 110868. doi: 10.1016/j.jenvman.2020.110868.

[22] Revellame, E.D., Fortela, D.L., Sharp, W., & Zappi, M.E. (2020). Adsorption kinetic modeling using pseudo-first order and pseudo-second order rate laws: A review. *Cleaner Engineering and Technology*, 1, article number 100032. doi: 10.1016/j.clet.2020.100032.

[23] Rudenko, V., Ivanenko, I., Kosogina, I., & Burmak, A. (2021). New efficient carbon adsorbent for water deironing. *Bulletin of Cherkasy State Technological University*, 26(1), 144-154. doi: 10.24025/2306-4412.1.2021.225318.

[24] Somyanonthanakun, W., Ahmed, R., Krongtong, V., & Thongmee, S. (2023). Studies on the adsorption of Pb(II) from aqueous solutions using sugarcane bagasse-based modified activated carbon with nitric acid: Kinetic, isotherm and desorption. *Chemical Physics Impact*, 6, article number 100181. doi: 10.1016/j.chphi.2023.100181.

[25] Tamarkina, Yu.V., Anishchenko, V.M., Redko, A.M., & Kucherenko, V.O. (2020). Adsorption properties of coals activated with potassium hydroxide. Influence of coal rank. *Chemistry, Physics and Technology of Surface*, 11(2), 175-189. doi: 10.15407/hftp11.02.175.

[26] Tamarkina, Yu.V., Anishchenko, V.M., Redko, A.M., & Kucherenko, V.O. (2022). Alkali activated coals. Microporous structure and capability to adsorb phenol compounds. *Chemistry, Physics and Technology of Surface*, 13(1), 111-124. doi: 10.15407/hftp13.01.111.

[27] Thommes, M., Kaneko, K., Neimark, A.V., Olivier, J.P., Rodriguez-Reinoso, F., Rouquerol, J., & Sing, K.S.W. (2015). Physisorption of gases, with special reference to the evaluation of surface area and pore size distribution (IUPAC Technical Report). *Pure and Applied Chemistry*, 87(9-10), 1051-1069. doi: 10.1515/pac-2014-1117.

[28] Wang, J., & Guo, X. (2022). Rethinking of the intraparticle diffusion adsorption kinetics model: Interpretation, solving methods and applications. *Chemosphere*, 309(2), article number 136732. doi: 10.1016/j.chemosphere.2022.136732.

[29] Wolak, E., & Orzechowska-Zięba, A. (2024). Change of the surface and structure of activated carbon as a result of HNO_3 modification. *Adsorption*, 30, 121-128. doi: 10.1007/s10450-023-00401-2.

[30] Zhu, S., Xu, J., Xie, J., Zhang, Z., Ding, Q., & Chen, K. (2024). Ultrafast dyeing wastewater purification by high-performance and reusable lignin-derived activated porous carbon filter. *Separation and Purification Technology*, 349, article number 127672. doi: 10.1016/j.seppur.2024.127672.

Адсорбенти з вугілля, окисненого азотною кислотою та активованого гідроксидом калію

Володимир Кучеренко

Доктор хімічних наук, старший науковий співробітник
Інститут фізико-органічної хімії і вуглехімії ім. Л.М. Литвиненка Національної академії наук України
02155, Харківське шосе, 50, м. Київ, Україна
https://orcid.org/0000-0001-7234-947X

Юлія Тамаркіна

Кандидат хімічних наук, старший науковий співробітник
Інститут фізико-органічної хімії і вуглехімії ім. Л.М. Литвиненка Національної академії наук України
02155, Харківське шосе, 50, м. Київ, Україна
https://orcid.org/0000-0002-8747-4481

Анастасія Редько

Провідний інженер
Інститут фізико-органічної хімії і вуглехімії ім. Л.М. Литвиненка Національної академії наук України
02155, Харківське шосе, 50, м. Київ, Україна
https://orcid.org/0000-0001-9768-4020

Ірина Фролова

Кандидат хімічних наук, науковий співробітник
Інститут фізико-органічної хімії і вуглехімії ім. Л.М. Литвиненка Національної академії наук України
02155, Харківське шосе, 50, м. Київ, Україна
https://orcid.org/0000-0001-9660-5474

Анотація. Найбільш ефективним методом отримання вуглецевих адсорбентів з високорозвиненою поверхнею (⩾1 000 м^2/г) є лужна активація. Її головний недолік – необхідність використання великих кількостей лугу – робить актуальним дослідження, спрямовані на удосконалення процессу. Мета роботи – кількісно оцінити вплив азотнокислотного окиснення довгополуменевого вугілля на пористу структуру та адсорбційні властивості адсорбентів, отриманих лужною активацією при невеликому співвідношенні KOH/вугілля (⩽1 г/г). У дослідженні використано експериментальний, аналітичний та порівняльний методи наукового пізнання. Характеристики адсорбентів отримано за даними інфрачервоної спектроскопії, порометрії, кінетики та ізотерм адсорбції 4-хлофенолу, барвника метиленового блакитного та катіонів свинцю з водних розчинів (25°C). Встановлено, що попереднє окиснення вугілля азотною кислотою утворює у вугільному каркасі етерні, естерні, фенольні, карбоксильні і нітрогрупи, що обумовлює приріст ваги вугілля до 16 % та істотно впливає на формування адсорбентів. Збільшення співвідношення HNO_3/карбон вугілля з 0 до 1,0 моль/моль зменшує вихід адсорбенту (з 50,2 % до 33,85 %), підвищує питому площу поверхні (з 1 685 м^2/г до 2 216 м^2/г) та на 25-51 % покращує адсорбційні властивості. Домінуюча частина (~80 %) впливу відбувається в інтервалі ⩽0,4 моль/моль. Порівнянням характеристик пористої структурі адсорбентів встановлено, що окиснення найбільше сприяє утворенню субнанопор і мезопор з діаметром 2-5 нм. Зіставленням адсорбційних властивостей визначено, що адсорбенти з окисненого вугілля адсорбують більшу кількість адсорбатів (в 1,20-1,43 рази) з більшою початковою швидкістю (в 1,2-4,0 рази). Ця властивість адсорбенту дуже важлива для термінового очищення води від високотоксичних сполук. Адсорбент з окисненого вугілля має розвиненішу поверхню і субнанопористу структуру та є більш адсорбційно активним ніж матеріал з неокисненого вугілля. Попереднє окиснення дозволяє суттєво збільшити адсорбційну здатність активованого вугілля вловлювати екотоксиканти з водних середовищ

Ключові слова: оксивугілля; лужний термохемоліз; пористий вуглецевий матеріал; пориста структура; поглинання екотоксикантів